Conductive polymer nanoantennas for dynamicorganic plasmonics

Shangzhi Chen, Evan S. H. Kang, Mina Shiran Chaharsoughi, Vallery Stanishev, Philipp Kuhne, Hengda Sun, Chuanfei Wang, Mats Fahlman, Simone Fabiano, Vanya Darakchieva and Magnus Jonsson

Chen, S., Kang, E. S. H., Shiran Chaharsoughi, M., Stanishev, V., Kuhne, P., Sun, H., Wang, C., Fahlman, M., Fabiano, S., Darakchieva, V., Jonsson, M., (2020), Conductive polymer nanoantennas for dynamicorganic plasmonics, *Nature Nanotechnology*, 15, . https://doi.org/10.1038/s41565-019-0583-y

Original publication available at:
https://doi.org/10.1038/s41565-019-0583-y

Conductive Polymer Nanoantennas for Dynamic Organic Plasmonics

Shangzhi Chen[1], Evan S. H. Kang[1], Mina Shiran Chaharsoughi[1], Vallery Stanishev[2], Philipp Kühne[2], Hengda Sun[1], Chuanfei Wang[1], Mats Fahlman[1], Simone Fabiano[1], Vanya Darakchieva[2] and Magnus P. Jonsson[1]*

[1]Laboratory of Organic Electronics, Department of Science and Technology (ITN), Linköping University, SE-601 74 Norrköping, Sweden. [2]Terahertz Materials Analysis Center (THeMAC) and Center for III-N Technology, C3NiT – Janzèn, Department of Physics, Chemistry and Biology (IFM), Linköping University, SE-581 83 Linköping, Sweden. *e-mail: magnus.jonsson@liu.se

Being able to dynamically shape light at the nanoscale is one of the ultimate goals in nanooptics[1]. Resonant light-matter interaction can be achieved using conventional plasmonics based on metal nanostructures, but their tunability is highly limited due to fixed permittivity[2]. Materials with switchable states and methods for dynamic control of light-matter interaction at the nanoscale are therefore desired. Here we show that nanodisks of a conductive polymer can support localised surface plasmon resonances in the near-infrared and function as dynamic nanooptical antennas, with their resonance behaviour tuneable by chemical redox reactions. These plasmons originate from the mobile polaronic charge carriers of a poly[3,4-ethylenedioxythiophene:sulfate (PEDOT:Sulf) polymer network. We demonstrate complete and reversible switching of the optical response of the nanoantennas by chemical tuning of their redox state, which modulates the material permittivity between plasmonic and dielectric regimes via non-volatile changes in the mobile charge carrier density. Further research may study different conductive polymers and nanostructures and explore their use in various applications, such as dynamic metaoptics and reflective displays.

We prepared thin conductive polymer films of poly[3,4-ethylenedioxythiophene:sulfate] (PEDOT:Sulf, see Fig. 1a), which can provide high electrical conductivity and metallic character[3,4]. Using vapour phase polymerization and sulfuric acid treatment (see Methods), we obtained films with electrical conductivity exceeding 5000 S/cm (see Supplementary Table. 1). Their complex and anisotropic permittivity was determined by ultrawide spectral range ellipsometry, employing an anisotropic Drude-Lorentz model as described previously (see Supplementary Table. 2)[5]. Fig. 1b shows the resulting in-plane permittivity of a thin PEDOT:Sulf film with thickness of 32 nm (Supplementary Fig. 1 presents the raw data). The shaded area highlights a spectral region (0.8 to 3.6 μm) in which the film has negative real permittivity and lower magnitude imaginary permittivity, which we define as plasmonic regime. This optically metallic and plasmonic character is related to the high conductivity within the thin film due to high concentration (2.6×10^{21} cm^{-3}, determined by ellipsometry, see Supplementary Table. 1 and Supplementary Information for details) of mobile positive polaronic charge carriers. We also note that the mobility is highly anisotropic[5,6] and the out-of-plane real permittivity (Supplementary Fig. 2a) is primarily positive throughout the measured range, making the conductive polymer thin film a natural hyperbolic material[7] (Supplementary Fig. 3).

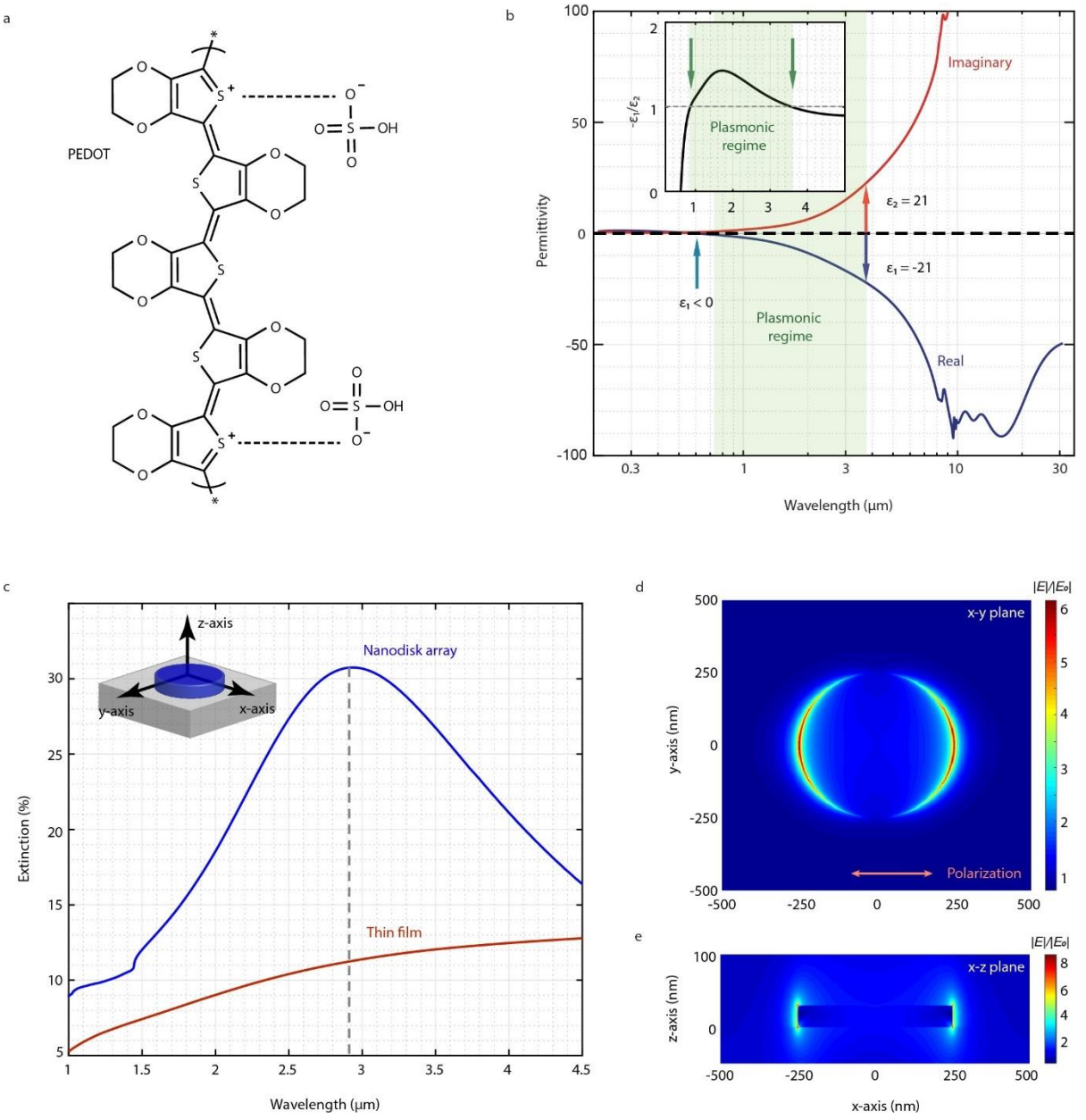

Fig. 1 | Material properties and calculated plasmonic resonances for PEDOT:Sulf in its high-conductivity oxidised state. a, Chemical structure of PEDOT:Sulf. **b,** In-plane permittivity dispersion of PEDOT:Sulf in its oxidised state (blue curve: real part; red curve: imaginary part). The shaded spectral range between 0.8 to 3.6 μm is defined as plasmonic regime where the real permittivity is below zero and its magnitude is larger than the imaginary component [inset: Negative ratio of the real and imaginary permittivity $(-\varepsilon_1/\varepsilon_2)$]. **c,** Simulated extinction spectrum for a PEDOT:Sulf nanodisk array (blue curve), with disk thickness of 30 nm, diameter of 500 nm, and array period of 1000 nm. The small extinction kink at about 1.4 μm disappears when examining single nanodisks instead of arrays (Fig. S4) and is attributed to lattice scattering of the array (see Fig. S5a). The red curve shows the extinction for a non-structured thin PEDOT:Sulf film scaled to the same material coverage as the disks (scaled by π/16). Inset: a schematic illustration of a PEDOT:Sulf nanodisk on a glass substrate with *x*-, *y*-, and *z*-axes indicated. **d, e,** Calculated nearfield profiles at the wavelength of the extinction maximum (2.9 μm) for one of the PEDOT:Sulf nanodisks of the array in **c** (mesh size: 1×1×1 nm^3 around the nanodisk): **d**, *x*-*y* in-plane direction 2 nm above the nanodisk; **e**, *x*-*z* cross-section through the center of the nanodisk. The colour scale bars show the electric field strength relative to the incident light ($|E|/|E_0|$).

The measured optical properties of the thin PEDOT:Sulf film imply that nanostructures of the material should be able to sustain plasmonic resonances. Indeed, the calculated optical

extinction (see Methods for details) for a PEDOT:Sulf nanodisk array (thickness of 30 nm, nanodisk diameter of 500 nm and array period of 1000 nm) shows a clear resonance peak at around 2.9 μm (Fig. 1c), which is absent for the non-structured thin film. Examining the optical nearfield profile at resonance (2.9 μm) for one of the nanodisks reveals that the extinction peak originates from a dipolar mode (Fig. 1d and e), with enhanced fields on the opposite edges of the nanodisk in the polarization direction of the incident light. The optical nearfield patterns slightly above (Fig. 1d) and through the nanodisk (Fig. 1e) both resemble that of traditional gold nanodisk antennas (comparison in Supplementary Fig. 4). Varying the array period for fixed nanodisk dimensions did not significantly shift the resonance wavelength (Supplementary Fig. 5b), confirming that the extinction peak originates from localized nanooptical modes rather than grating effects. In fact, also single nanodisks (Supplementary Fig. 6a) show the same nanooptical behaviour, with almost identical resonance positions as the periodic arrays (Supplementary Fig. 6b), and without the small grating-induced kink at shorter wavelengths as present for the periodic arrays (see Supplementary Fig. 5). To verify the plasmonic character of the resonance, we also evaluated the optical response for nanodisks made from an artificial material with permittivity originating only from the polaronic charge carriers ("Transport function", see Supplementary Fig. 7b and Supplementary Information section B7 for details). Those nanodisks exhibit an extinction resonance peak with even higher intensity and smaller width compared with the response of the original nanodisks (see Supplementary Fig. 7b). We thereby conclude that the nanooptical resonance originates primarily from the mobile charge carriers in the conducting polymer and that it is plasmonic in character (see more detailed discussion in Supplementary Information section B8).

To experimentally verify excitation of plasmons in conductive polymer nanostructures, we fabricated short-range ordered arrays of PEDOT:Sulf nanodisks on sapphire substrates, using a modified version of colloidal lithography[8] (see Methods and Supplementary Fig. 8 for details). The protocol could provide large areas of nanodisks of desired diameters, visualized by atomic force microscopy (AFM) for nanodisk diameters of 120 nm, 280 nm, and 710 nm in Fig. 2a, b, and c, respectively (more AFM images and line sections of single nanodisks are provided in Supplementary Fig. 9). The nanodisks all originate from 30 nm thick PEDOT:Sulf films, while the final thickness of the disks varied somewhat due to residual PMMA [poly(methyl methacrylate)] remaining on top of the disks after fabrication (Supplementary Fig. 10). Importantly, the fabricated polymer nanodisk samples exhibit clear extinction peaks (Fig. 2d, e, and f), verifying the simulated nanooptical behaviour. As expected for plasmonic nanoantennas, the resonance positions increase with disk diameter. The experimental results largely match the simulated predictions (Fig. 2g, h, and i) in terms of spectral shapes, peak widths and resonance wavelengths. Small differences in peak positions are attributed to geometrical differences and imperfections of the fabricated nanodisks. The experimental peaks also show somewhat larger broadening, as expected for measured ensembles compared with simulated arrays composed of identical nanostructures[9].

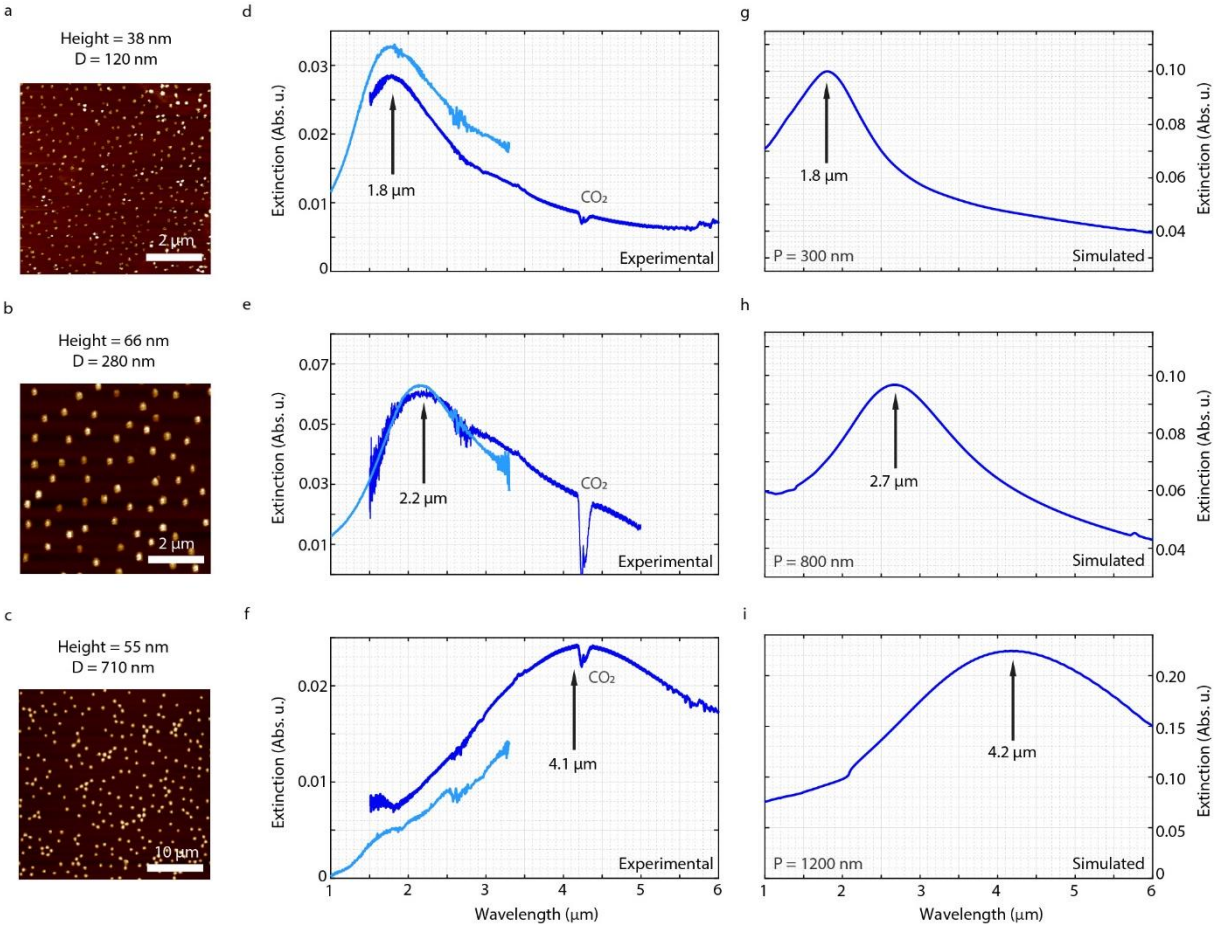

Fig. 2 | Extinction spectra of PEDOT:Sulf nanodisk antennas. Three different sizes of short-range ordered nanodisk arrays were made on sapphire substrates: **a**, AFM image of 120 nm diameter nanodisks; **b**, AFM image of 280 nm diameter nanodisks; **c**, AFM image of 710 nm diameter nanodisks. The diameter and height measurements are in **Supplementary Fig. 9**. **d**, **e**, and **f**, Experimental measured extinction spectra of 120 nm, 280 nm, and 710 nm diameter nanodisks. UV-Vis-NIR measurements are plotted in light blue and FTIR measurements are in dark blue. **g**, **h**, and **i**, Simulated extinction spectra of 120 nm, 280 nm, and 710 nm diameter nanodisk arrays. In the simulation, the PEDOT:Sulf thickness was 30 nm and the excessive thickness (8 nm, 36 nm, and 25 nm respectively) comes from remaining unremoved PMMA layer. The features between 2.7 µm and 3.3 µm (with multiple closely-packed sharp peaks) and at 4.3 µm in the experimental spectra (d, e, and f) are due to absorption by water vapour and carbon dioxide[10], respectively, and therefore absent in the simulated spectra.

The results above indicate that the resonance position of the polymer nanodisk antennas can be tuned by geometry. Fig. 3a presents the simulated extinction for 30 nm thick single PEDOT:Sulf nanodisks of varying diameter on a substrate with refractive index of 1.6. Normalized extinction versus diameter is presented in Fig. 3c as colour maps. It is clear that the resonance position redshifts with increasing diameter, enabling tuning in a large spectral range from around 2 µm to around 4 µm for disks with sizes ranging from 200 nm and 700 nm in diameter. The spectral tunability can likely be extended further by other geometries. While the nanodisk resonances redshift with increasing disk diameter, they instead blueshift with increasing thickness, as presented in Fig. 3d and 3f for nanodisks with fixed diameter of 500 nm (normalized extinction spectra corresponding to Fig. 3a and 3d are shown in Supplementary Fig. 11). Both these geometrical dependencies match expectations based on plasmonic nanodisk resonances[11-13].

To enable analytical calculation of the optical response, we approximate the nanodisks as oblate spheroids with diameter *D* and thickness *t*, which in the quasi-static limit $D \ll \lambda$ gives the dipolar polarizability α as[2]

$$\alpha(\lambda) = V \frac{\varepsilon(\lambda) - \varepsilon_s}{\varepsilon_s + L[\varepsilon(\lambda) - \varepsilon_s]} \quad (1)$$

where *V* is the volume of the spheroid and ε_s is the permittivity of the surrounding medium. We use the in-plane permittivity of PEDOT:Sulf as $\varepsilon(\lambda)$ and set ε_s = 1.69 as the effective surrounding permittivity for disks in air on a substrate with refractive index 1.6 (see Methods). *L* is a geometrical factor that equals 1/3 for a sphere (*D* = *t*) and decreases for increasing nanodisk ratio (*D* > *t*, see Supplementary Fig. 12). To fulfil the resonance condition of maximum polarizability when *L* decreases, the magnitude of the negative permittivity needs to increase. Because the permittivity of the conductive polymer increases in magnitude with wavelength (see Fig. 1b), the resonance position therefore redshifts with increasing aspect ratio (*D*/*t*). This illustrates why the resonance of the PEDOT:Sulf nanoantennas redshifts with increasing disk diameter and blueshifts with increasing disk thickness. Larger disks require corrections for finite wavelength effects, which gives the corrected polarizability as[14,15]

$$\alpha'(\lambda) = \alpha(\lambda)\left[1 - \frac{k^2}{2\pi D}\alpha(\lambda) - i\frac{k^3}{6\pi}\alpha(\lambda)\right] \quad (2)$$

where *k* is the wave number of the incident light. The extinction cross-section $\sigma(\lambda)$ can now be calculated *via*[2]

$$\sigma(\lambda) = k\mathrm{Im}[\alpha'(\lambda)] \quad (3)$$

Fig. 3b and 3e show the final calculated extinction cross sections of single PEDOT:Sulf oblate spheroids, with sizes corresponding to the simulated nanodisks in Fig. 3a and 3d, respectively. The calculated results based on the dipolar polarizability match the results from the full simulations quite well, both in terms of extinction magnitude and its increase with aspect ratio, and in terms of peak positions and their redshift with increasing nanodisk aspect ratio. The results thereby further corroborate that the observed extinction peaks of the PEDOT:Sulf nanodisks originate from dipolar plasmonic excitations. However, while the presented organic plasmonic systems provide optical behaviour similar to conventional plasmonic systems, they are different in that the plasmons are based on collective oscillations of mobile polaronic charge carriers, including bipolarons formed by coupling of positive charge pairs and local chain distortions[16].

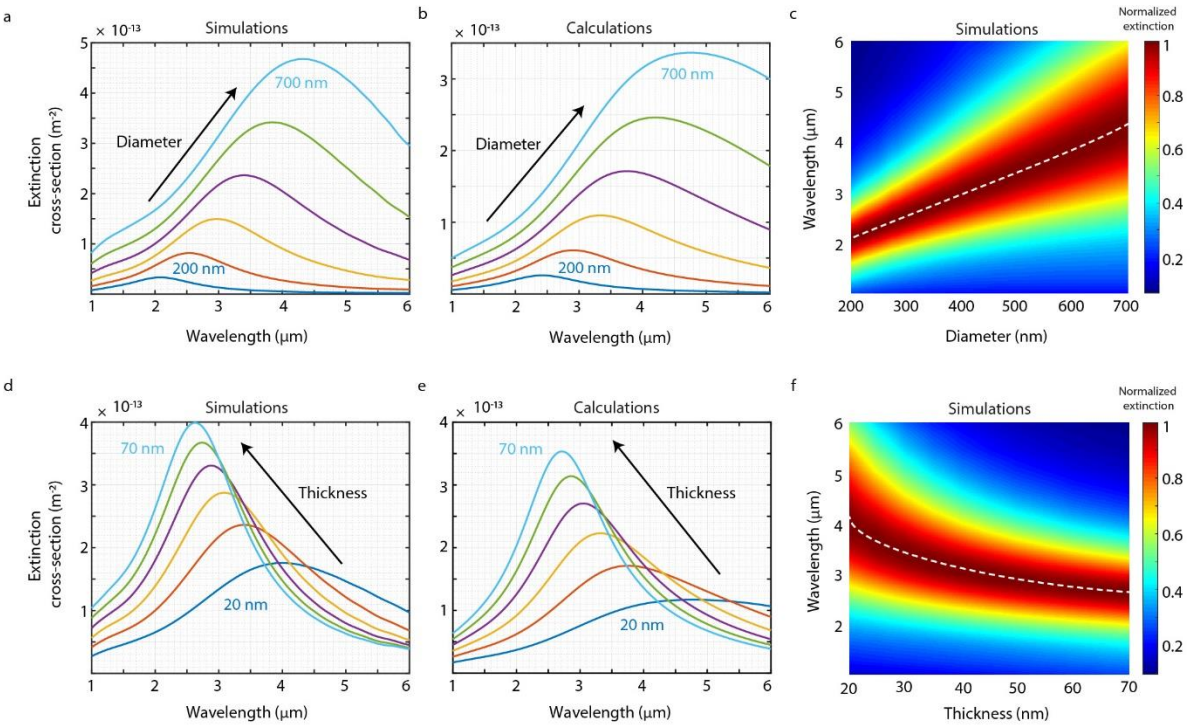

Fig. 3 | Geometry dependence of single PEDOT:Sulf nanodisk localized plasmons. a, Simulated extinction cross-section of 30 nm thick single nanodisks of different diameters (diameter step size = 100 nm, substrate refractive index = 1.6). **b**, Analytically calculated extinction cross-section for oblate spheroids corresponding to the nanodisk sizes in **a**. **c**, Colour map of simulated normalized extinction versus diameter for single 30 nm thick nanodisks. **d**, Simulated extinction cross-section of 500 nm in diameter single nanodisks with different thickness (thickness step size = 10 nm, substrate refractive index = 1.6). **e**, Analytically calculated extinction cross section for oblate spheroids corresponding to the nanodisk sizes in **d**. **c**, Colour map of simulated normalized extinction versus diameter for single 30 nm thick nanodisks. **f**, Colour map of simulated normalized extinction versus thickness for single 500 nm in diameter nanodisks. The white dashed lines in **c** and **f** indicate the resonance peak position and its shift with changes in diameter and thickness, respectively. The colour scale bars in **c** and **f** present the normalized extinction. See **Supplementary Fig. 11** for normalized extinction spectra corresponding to **a** and **d**.

Finally, we demonstrate that the conductive polymer nanoantennas can be switched on and off. Among various approaches to tune nanophotonic systems, recent research has explored tuning by modulating the free charge carriers in plasmonic systems, including electrical gating[17] and photo-carrier excitation[18]. While this approach is rather limited for traditional plasmonic materials, conductive polymers hold great promise since their polaronic charge carrier concentration can be modulated by several orders of magnitude *via* their redox state[19]. Here, we control the redox state chemically, by exposing PEDOT:Sulf to the vapour of a highly branched poly(ethylenimine) (PEI, see chemical structure in left panel of Fig. 4a). PEI contains volatile amines, such as ethyleneimine dimers and trimers, that are known to effectively reduce PEDOT as well as other semiconducting materials[20]. Optical extinction spectroscopy of a (non-structured) thin PEDOT:Sulf films visualizes the process *via* almost complete reduction of the free charge carrier absorption in the IR and the emergence of a neutral state peak at around 600 nm (see Fig. 4b)[20]. For the reduced polymer, PEI reduces the polaronic charge carrier concentration in PEDOT by donating electrons to it, and complexing the Sulf counterions (see Supplementary Fig. 13b). This results in a material with largely reduced electrical conductivity (schematic mechanism in Fig. 4a right panel)[20]. The process is reversible and we can recover the original optical properties of the PEDOT film *via* acid

treatment of the reduced film (see Methods). This process re-oxidises the material, for which the neutral state disappears and the absorption returns to that of the initial pristine film (Fig. 4b). Knowing that the optical material properties of PEDOT:Sulf can be reversibly modulated, we utilize this feature to actively tune our polymer nanodisk metasurfaces. The black curve in Fig. 4c shows the extinction spectra of a sample with PEDOT:Sulf nanodisks in their oxidised pristine state, with plasmonic resonance peak at around 1900 nm. This peak completely disappears upon PEI vapour treatment, for which the material in the nanodisks is no longer plasmonic, due to drastic reduction of the polaronic charge carrier concentration. Indeed, the neutral state material absorption emerges at 600 nm for the PEI treated metasurfaces. Importantly, the optical properties are not volatile, but stable over time and we observe only minimal extinction changes of the sample after one week (see Supplementary Fig. 14). By re-oxidising the sample with sulfuric acid, the plasmonic resonance peak recovers to its initial state, with both similar intensity and width as for the original plasmonic metasurface (Fig. 4c). This process was also verified by X-ray photoelectron spectroscopy (XPS), which shows successful removal of PEI residues from the re-oxidised PEDOT:Sulf films (see Supplementary Fig. 13). We also note that the increase in extinction below 800 nm for the re-oxidised sample (Fig. 4c) is likely due to different probe areas combined with some polystyrene beads remaining after fabrication (similar effects were observed for samples before and after bead removal, Supplementary Fig. 15). Indeed, other samples did not show such increase in extinction for lower wavelengths after re-oxidisation (see Supplementary Fig. 16). We also note that some samples showed an initial decrease in peak intensity after the first on-off redox cycle (Supplementary Fig. 16), which may be due to some more loosely bound nanodisks being removed during the switching process. Differences in exact oxidation state before and after switching may also play a role. Importantly, the spectra rapidly stabilized after the initial cycles and the nanodisks could be repeatedly switched on and off for multiple cycles (here tested for in total 6 cycles).

We have demonstrated that nanodisks made of highly conductive polymers can function as optical nanoantennas to form active plasmonic metasurfaces. While previous research investigated hybrid systems based on the combination of metallic nanostructures and conductive polymers[21,22], the polymer itself here acts as the plasmonic material, without presence of any inorganic metals. Our research thereby expands the palette of materials for plasmonics beyond conventional metals and other recently explored materials, such as transparent conductive oxides[23], polycyclic aromatic hydrocarbons[24], and graphene[25]. The plasmonic behaviour of these nanoantennas is dynamically tuneable via the redox state of the conductive polymer, where future work may also explore electrochemical modulation or other means of dynamic control [26]. Besides improving the fundamental understanding of the intriguing physics of these nanoantenna systems, future work may explore their use in a multitude of areas, ranging from dynamic metaoptics and metatronics to plasmon-enhanced electrochemistry and reflective displays. To that end, the possibility to modify conductive polymers by side chain engineering[27] makes them versatile and may enable applications that are not feasible with conventional materials. These applications may also benefit from additional features of conductive polymers, including low cost, flexibility, bio-compatibility, and processability in solution[19]. The future also holds promise for conductive polymers with

yet further improved plasmonic properties, for example, based on strategies to improve electrical conductivity and lower defect density, such as by effective chain alignment[28] or sequential doping[29]. We hope that our study of redox-tuneable conductive polymer plasmonics will inspire research in this interdisciplinary field of manipulating light-matter interactions at the nanoscale.

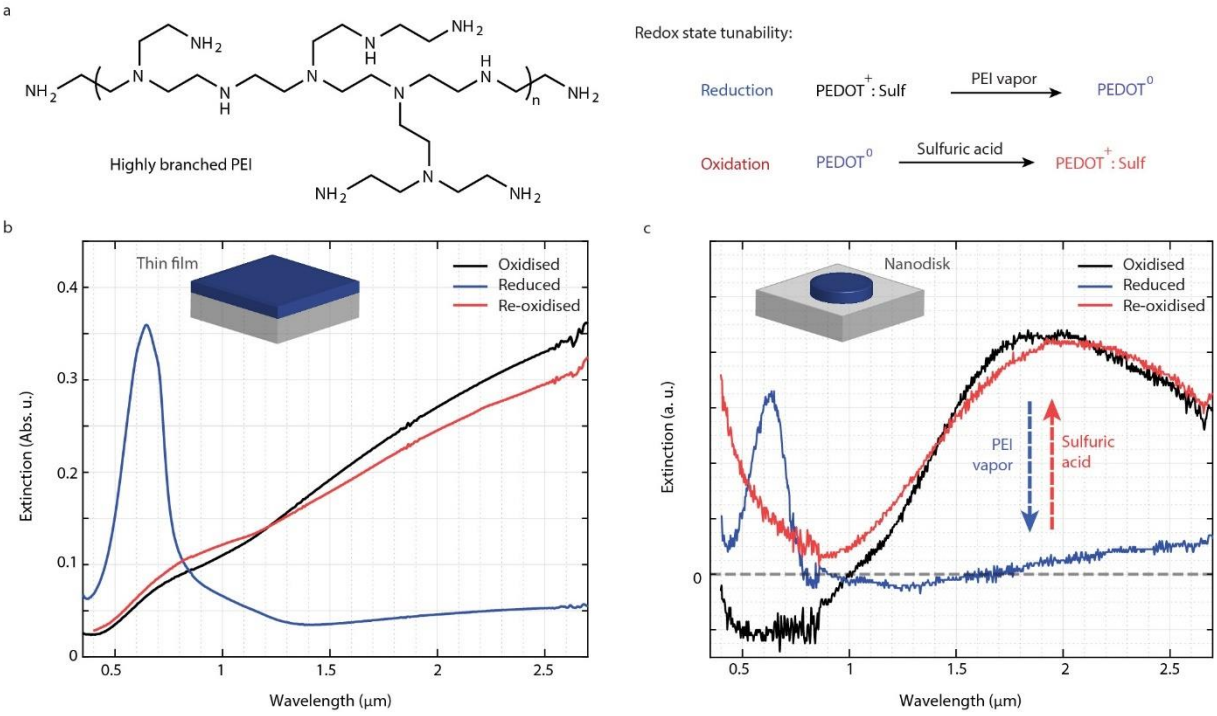

Fig. 4 | Redox state tunability of PEDOT:Sulf nanodisk antennas. a, Chemical structure of highly branched PEI (left panel) and redox state tunability mechanism for the PEDOT-based material (right panel). The plus sign (+) indicates that PEDOT is in its oxidised state, whereas 0 denotes PEDOT is in its reduced state. **b**, Measured extinction for thin PEDOT:Sulf film on glass at different redox states. **c**, Measured extinction for PEDOT:Sulf nanodisks on glass (thickness of 43 nm and nanodisk diameter of 140 nm) at different redox states.

References

1 Shaltout, A. M., Shalaev, V. M. & Brongersma, M. L. Spatiotemporal light control with active metasurfaces. *Science* **364**, eaat3100 (2019).

2 Maier, S. A. *Plasmonics: Fundamentals and Applications*. (Springer Science & Business Media, 2007).

3 Massonnet, N., Carella, A., de Geyer, A., Faure-Vincent, J. & Simonato, J.-P. Metallic behaviour of acid doped highly conductive polymers. *Chemical Science* **6**, 412-417 (2015).

4 Gueye, M. N. *et al.* Structure and dopant engineering in PEDOT thin films: Practical tools for a dramatic conductivity enhancement. *Chemistry of Materials* **28**, 3462-3468 (2016).

5 Chen, S. *et al.* On the anomalous optical conductivity dispersion of electrically conducting polymers: ultra-wide spectral range ellipsometry combined with a Drude–Lorentz model. *Journal of Materials Chemistry C* **7**, 4350-4362 (2019).

6 Aasmundtveit, K. E. *et al.* Structure of thin films of poly (3, 4-ethylenedioxythiophene). *Synthetic Metals* **101**, 561-564 (1999).

7 Poddubny, A., Iorsh, I., Belov, P. & Kivshar, Y. Hyperbolic metamaterials. *Nature Photonics* **7**, 948 (2013).

8 Hanarp, P., Käll, M. & Sutherland, D. S. Optical properties of short range ordered arrays of nanometer gold disks prepared by colloidal lithography. *The Journal of Physical Chemistry B* **107**, 5768-5772 (2003).
9 Stete, F., Koopman, W. & Bargheer, M. Signatures of strong coupling on nanoparticles: revealing absorption anticrossing by tuning the dielectric environment. *ACS Photonics* **4**, 1669-1676 (2017).
10 Larkin, P. *Infrared and Raman Spectroscopy: Principles and Spectral Interpretation*. (Elsevier, 2017).
11 Chang, W.-S. *et al.* Tuning the acoustic frequency of a gold nanodisk through its adhesion layer. *Nature Communications* **6**, 7022 (2015).
12 Fang, Z. *et al.* Active tunable absorption enhancement with graphene nanodisk arrays. *Nano Letters* **14**, 299-304 (2013).
13 Knight, M. W. *et al.* Aluminum for plasmonics. *ACS Nano* **8**, 834-840 (2013).
14 Langhammer, C., Yuan, Z., Zorić, I. & Kasemo, B. Plasmonic properties of supported Pt and Pd nanostructures. *Nano Letters* **6**, 833-838 (2006).
15 Wokaun, A., Gordon, J. P. & Liao, P. F. Radiation damping in surface-enhanced Raman scattering. *Physical Review Letters* **48**, 957 (1982).
16 Bredas, J. L. & Street, G. B. Polarons, bipolarons, and solitons in conducting polymers. *Accounts of Chemical Research* **18**, 309-315 (1985).
17 Lee, S. H. *et al.* Switching terahertz waves with gate-controlled active graphene metamaterials. *Nature Materials* **11**, 936 (2012).
18 Alam, M. Z., De Leon, I. & Boyd, R. W. Large optical nonlinearity of indium tin oxide in its epsilon-near-zero region. *Science* **352**, 795-797 (2016).
19 Kim, N. *et al.* in *Conjugated Polymers: Properties, Processing, and Applications.* (eds John R. Reynolds, Barry C. Thompson, & Terje A. Skotheim) Ch. 3 Electric Transport Properties in PEDOT Thin Films, 44-127 (CRC Press, 2019).
20 Fabiano, S. *et al.* Poly (ethylene imine) Impurities Induce n‐ doping Reaction in Organic (Semi) Conductors. *Advanced Materials* **26**, 6000-6006 (2014).
21 Jiang, N., Shao, L. & Wang, J. (Gold nanorod core)/(polyaniline shell) plasmonic switches with large plasmon shifts and modulation depths. *Advanced Materials* **26**, 3282-3289 (2014).
22 Jung, I. *et al.* Surface plasmon resonance extension through two-block metal-conducting polymer nanorods. *Nature Communications* **9**, 1010 (2018).
23 Li, S. Q. *et al.* Infrared plasmonics with indium–tin-oxide nanorod arrays. *ACS Nano* **5**, 9161-9170 (2011).
24 Lauchner, A. *et al.* Molecular plasmonics. *Nano Letters* **15**, 6208-6214 (2015).
25 Rodrigo, D. *et al.* Mid-infrared plasmonic biosensing with graphene. *Science* **349**, 165-168 (2015).
26 Mitraka, E. *et al.* Oxygen-induced doping on reduced PEDOT. *Journal of Materials Chemistry A* **5**, 4404-4412 (2017).
27 Mei, J. & Bao, Z. Side chain engineering in solution-processable conjugated polymers. *Chemistry of Materials* **26**, 604-615 (2013).
28 Xu, J. *et al.* Multi-scale ordering in highly stretchable polymer semiconducting films. *Nature Materials* **18**, 594 (2019).
29 Vijayakumar, V. *et al.* Bringing Conducting Polymers to High Order: Toward Conductivities beyond 105 S cm^{-1} and Thermoelectric Power Factors of 2 mW m^{-1} K^{-2}. *Advanced Energy Materials* **9**, 1900266 (2019).

Acknowledgements

The authors thankfully acknowledge financial support from the Swedish Research Council, the Swedish Foundation for Strategic Research, the Wenner-Gren Foundations, and the Swedish Government Strategic Research Area in Materials Science on Functional Materials at Linköping University (Faculty Grant SFO-Mat-LiU No. 2009 00971).

Author contributions

M.P.J. conceived and supervised the project. S.C., V.S., P.K., and V.D. performed ellipsometry measurements and data analysis. S.C. and M.S.C. fabricated the nanostructures. S.C., M.P.J. and E.S.H.K. performed numerical simulations. H.S. and S.C. performed PEI vapour treatments supervised by S.F. C. W. and M. F. performed XPS measurements and analysis. S.C performed all the other characterizations. S.C. and M.P.J. organized the data and wrote the manuscript. All authors reviewed and commented on the manuscript.

Competing interests

The authors declare no conflicts of interest.

Data availability

The data that support the plots within this paper and other findings of this study are available from the corresponding author upon reasonable request.

Additional information

Supplementary information is available in the online version of the paper. Reprints and permission information is available online at www.nature.com/reprints. Correspondence and requests for materials should be addressed to M.P.J.

Figure captions

Fig. 1 | Material properties and calculated plasmonic resonances for PEDOT:Sulf in its high-conductivity oxidised state. a, Chemical structure of PEDOT:Sulf. **b,** In-plane permittivity dispersion of PEDOT:Sulf in its oxidised state (blue curve: real part; red curve: imaginary part). The shaded spectral range between 0.8 to 3.6 µm is defined as plasmonic regime where the real permittivity is below zero and its magnitude is larger than the imaginary component [inset: Negative ratio of the real and imaginary permittivity $(-\varepsilon_1/\varepsilon_2)$]. **c,** Simulated extinction spectrum for a PEDOT:Sulf nanodisk array (blue curve), with disk thickness of 30 nm, diameter of 500 nm, and array period of 1000 nm. The small extinction kink at about 1.4 µm disappears when examining single nanodisks instead of arrays (Fig. S4) and is attributed to lattice scattering of the array (see Fig. S5a). The red curve shows the extinction for a non-structured thin PEDOT:Sulf film scaled to the same material coverage as the disks (scaled by π/16). Inset: a schematic illustration of a PEDOT:Sulf nanodisk on a glass substrate with *x*-, *y*-, and *z*-axes indicated. **d, e,** Calculated nearfield profiles at the wavelength of the extinction maximum (2.9 µm) for one of the PEDOT:Sulf nanodisks of the array in **c** (mesh size: 1×1×1 nm^3 around the nanodisk): **d**, *x*-*y* in-plane direction 2 nm above the nanodisk; **e**, *x*-*z* cross-section through the center of the nanodisk. The colour scale bars show the electric field strength relative to the incident light ($|E|/|E_0|$).

Fig. 2 | Extinction spectra of PEDOT:Sulf nanodisk antennas. Three different sizes of short-range ordered nanodisk arrays were made on sapphire substrates: **a**, AFM image of 120 nm diameter nanodisks; **b**, AFM image of 280 nm diameter nanodisks; **c**, AFM image of 710 nm diameter nanodisks. The diameter and height measurements are in **Supplementary Fig. 9**. **d**, **e**, and **f**, Experimental measured extinction spectra of 120 nm, 280 nm, and 710 nm diameter nanodisks. UV-Vis-NIR measurements are plotted in light blue and FTIR

measurements are in dark blue. **g**, **h**, and **i**, Simulated extinction spectra of 120 nm, 280 nm, and 710 nm diameter nanodisk arrays. In the simulation, the PEDOT:Sulf thickness was 30 nm and the excessive thickness (8 nm, 36 nm, and 25 nm respectively) comes from remaining unremoved PMMA layer. The features between 2.7 µm and 3.3 µm (with multiple closely-packed sharp peaks) and at 4.3 µm in the experimental spectra (d, e, and f) are due to absorption by water vapour and carbon dioxide[10], respectively, and therefore absent in the simulated spectra.

Fig. 3 | Geometry dependence of single PEDOT:Sulf nanodisk localized plasmons. a, Simulated extinction cross-section of 30 nm thick single nanodisks of different diameters (diameter step size = 100 nm, substrate refractive index = 1.6). **b**, Analytically calculated extinction cross-section for oblate spheroids corresponding to the nanodisk sizes in **a**. **c**, Colour map of simulated normalized extinction versus diameter for single 30 nm thick nanodisks. **d**, Simulated extinction cross-section of 500 nm in diameter single nanodisks with different thickness (thickness step size = 10 nm, substrate refractive index = 1.6). **e**, Analytically calculated extinction cross section for oblate spheroids corresponding to the nanodisk sizes in **d**. **c**, Colour map of simulated normalized extinction versus diameter for single 30 nm thick nanodisks. **f**, Colour map of simulated normalized extinction versus thickness for single 500 nm in diameter nanodisks. The white dashed lines in **c** and **f** indicate the resonance peak position and its shift with changes in diameter and thickness, respectively. The colour scale bars in **c** and **f** present the normalized extinction. See **Supplementary Fig. 11** for normalized extinction spectra corresponding to **a** and **d**.

Fig. 4 | Redox state tunability of PEDOT:Sulf nanodisk antennas. a, Chemical structure of highly branched PEI (left panel) and redox state tunability mechanism for the PEDOT-based material (right panel). The plus sign (+) indicates that PEDOT is in its oxidised state, whereas 0 denotes PEDOT is in its reduced state. **b**, Measured extinction for thin PEDOT:Sulf film on glass at different redox states. **c**, Measured extinction for PEDOT:Sulf nanodisks on glass (thickness of 43 nm and nanodisk diameter of 140 nm) at different redox states.

Methods

Thin film deposition. PEDOT:trifluoromethanesulfonate (PEDOT:OTf) thin films were prepared first as precursors of PEDOT:Sulf films. PEDOT:OTf thin films were deposited *via* vapour phase polymerization (VPP) as reported in the literature.[5,30] The oxidant solution for EDOT polymerization was prepared by mixing 0.03 g of iron (III) trifluoromethanesulfonate (Fe[OTf]3, from Alfa Aesar), 0.2 g of tri-block co-polymer poly(ethylene glycol)-block-poly(propylene glycol)-block-poly(ethylene glycol) (PEG-PPG-PEG or P-123, average M_n ~5,800, from Sigma-Aldrich) and 0.8 g of 99.5% ethanol (from Solveco). Oxidant films were deposited by spin-coating at 1500 rpm for 30 s onto pre-cleaned sapphire or glass substrates (sonicated in cleaning detergent, de-ionized water, acetone, and isopropanol each for 10 min respectively and treated with oxygen-plasma at 200 W for 5 min before use). After 30 s baking on a hotplate at 70 °C, the samples were transferred into a heated vacuum desiccator [Vacuo-temp, from SELECTA]. EDOT (142.18 g mol^{-1}, from Sigma-Aldrich) droplets were drop-casted onto a glass substrate on a hot plate at 30 °C in the desiccator to ensure its evaporation. After 30 min of polymerization at a pressure of 70 mBar, the samples were taken out from the desiccator and washed with ethanol multiple times to remove byproducts and unreacted residues, followed by air-drying with nitrogen. To further enhance the electrical properties of the samples, we used an acid treatment by soaking the samples in 1 M sulfuric acid (H_2SO_4) for 10 min at room temperature followed by washing in DI water for 10 seconds and heating at 100 °C for another 10 min[30]. Upon acid treatment, the OTf counterions in the PEDOT:OTf films were replaced by sulfate counterions (HSO_4^-), as clear from the removal of fluorine signals in X-ray photoelectron spectroscopy results (XPS, see Supplementary Fig. 14a).

Nanoantenna fabrication. The detailed process flow for nanodisk array fabrication is shown in Supplementary Fig. 8, which is a modified version of colloidal lithography.[8] Briefly, a 4 wt% PMMA [poly(methyl methacrylate)], M_w ~ 996,000, from Sigma-Aldrich) solution in anisole (from Sigma Aldrich) was spin-coated onto the as-prepared PEDOT:Sulf thin films. Soft baking at 140 °C for 10 min was then applied. The samples were treated with reactive oxygen plasma (50 W, 250 mTorr) for 5 s to increase the hydrophilicity of the surface. In order to functionalize the PMMA surface to be positively charged, 2 wt% poly(diallyldimethylammonium chloride) (PDDA, 522376 from Sigma-Aldrich) in DI water was dropped on the samples. After 1 min, the samples were rinsed with deionized water for 40 s and dried with nitrogen stream. Negatively charged polystyrene nanoparticles (PS beads with different diameters, 0.2-0.3 wt% in deionized water, from Microparticles GmbH) were then dropped on the samples. After 10-30 min, the samples coated with PS beads were rinsed with DI water and dried with nitrogen stream resulting in a sparse monolayer of PS beads on the PMMA/PEDOT:Sulf thin films. A heat treatment at 100 °C for 2 min were applied to the samples to improve the adhesion of PS beads on the samples. Reactive oxygen plasma etching (250 mTorr, 50 W) for 3-5 min were applied to the samples, using the PS beads monolayer as mask. Depending on the size of PS beads and thickness of PMMA and PEDOT:Sulf thin films, the time interval of etching can be varied to ensure a complete removal of PMMA and PEDOT:Sulf parts that are not covered by the mask. The samples were then placed into an acetone bath and soaked for 10-30 min followed by a mild sonication for 3 min and nitrogen stream drying to remove PMMA and PS beads and finally the PEDOT:Sulf nanodisks were obtained. In this study, three different diameters of PS beads were used: 239 nm (PS-ST-0.25, Microparticles GmbH), 497 nm (PS-ST-0.50, Microparticles GmbH), and 1046 nm (PS-ST-1.0, Microparticles GmbH).

Vapour treatment of thin films and nanoantennas. The vapour treatment was conducted inside a N_2-filled glovebox by exposing the samples to the vapour of ethyleneimine dimers and trimers by heating a vial containing highly branched poly(ethylene imine) liquid (PEI, M_w ~ 800, from Sigma-Aldrich) at 120 °C for 5 min.[20] After the vapour treatment, the samples were annealed at 120 °C for another 5 min.

To re-oxidise the samples, they were put into 1 M sulfuric acid bath for 10 min followed by a drying process of 10 min at 100 °C on a hot plate.

Ellipsometry. PEDOT:Sulf thin film samples were measured at normal ambient conditions at room temperature. The films were deposited on 2-inch single side polished *c*-plane sapphire wafers (from Semiconductor Wafer Inc.). Ellipsometric data for PEDOT:Sulf thin films were collected using three different ellipsometers covering a wide spectral range from 0.0028 eV to 5.9 eV. UV-Vis-NIR measurements were performed on a J. A. Woollam Co. RC2® spectroscopic ellipsometer for five incident angles (40°, 50°, 60°, 70°, and 80°) and spectral range from 0.73 eV (1690 nm) to 5.90 eV (210 nm). Infrared measurements were performed on a J. A. Woollam Co. IR-VASE® spectroscopic ellipsometer for two incident angles (50° and 70°) and spectral range from 28.0 meV (230 cm^{-1}) to 1.0 eV (7813 cm^{-1}). THz measurements were performed on the THz ellipsometer at the Terahertz Materials Analysis Center (THeMAC) at Linköping University.[31] Three incident angles (40°, 50°, and 60°) were used for THz measurements, in the spectral range between 2.8 meV (0.67 THz) and 4.0 meV (0.97 THz). The typical ellipsometer measures the complex reflectance ratio ρ at different frequencies, as obtained from $\rho = r_p/r_s = tan(\Psi)e^{i\Delta}$, where r_p and r_s are the complex Fresnel reflection coefficients for p- and s-polarized light; Ψ shows the amplitude ratio change of the two polarizations; and Δ indicates the phase difference between them.[32] WVASE® (J. A. Woollam Co.) software was used for data analysis and an anisotropic Drude-Lorentz model was employed for model fitting and optical parameter extraction for the PEDOT:Sulf thin films.[5] Details for data analysis were described in Supplementary Information.

Electrical, chemical and structural characterization. Sheet resistance, R_s, of the thin film was measured using a 4-point probe set-up using a Signatone Pro4 S-302 resistivity stand and a Keithley 2400. Film thickness *t* was determined by a surface profiler (Dektak 3st, Veeco). The thickness of the PEDOT:Sulf films varied in the range from 30 to 40 nm. The electrical conductivity can then be calculated by $\sigma = 1/(R_s t)$. Atomic force microscopy (AFM) was employed for surface morphology characterization, in tapping mode using a Veeco Dimension 3100. The morphological images were analysed using Nanoscope Analysis software (Bruker). X-ray Photoemission experiments were carried out using a Scienta ESCA 200 spectrometer under ultrahigh vacuum conditions at a base pressure of 1×10^{-10} mbar. The XPS measurements have been done with a monochromatic Al Kα X-ray source, providing photons with energy of 1,486.6 eV. The XPS spectra are normalized to the C1s peak.

Optical characterization. The extinction spectra in the Vis-NIR range (400 nm to 3300 nm) were measured using a UV-Vis-NIR spectrometer (Lambda 900, Perkin Elmer Instruments). The extinction spectra include transmission losses due to both absorption and scattering. Fourier-transform infrared spectroscopy (FTIR) measurements were performed in the spectral range from 1333 nm (7500 cm^{-1}) to 5000 nm (2000 cm^{-1}) or 6667 nm (1500 cm^{-1}) using an Equinox 55 spectrometer (Bruker). FTIR spectra were acquired in absorbance mode using a resolution 4 cm^{-1} and 100 scans. Samples deposited on 20×20×0.5 mm double-side polished sapphire substrates (from Semiconductor Wafer Inc.) were made for FTIR and UV-Vis-NIR measurements.

Optical numerical simulations. Numerical simulations (electric nearfield intensity and farfield spectra) of the electromagnetic response of PEDOT:Sulf nanoantennas were performed *via* the finite-difference time-domain (FDTD) method using the commercial software Lumerical FDTD Solutions (http://www.lumerical.com/fdtd.php). The optical parameters for the PEDOT:Sulf thin film were taken as the anisotropic complex permittivity obtained from the ellipsometry measurements. For periodic nanodisk arrays and thin films, the spectra and nearfield profiles were recorded *via* field and power monitors. Periodic PEDOT:Sulf nanodisk arrays (or thin film) were placed on top of glass or sapphire substrates. The structures were illuminated by a planewave light source at normal incidence. Anti-symmetrical and symmetric boundaries were used for the *x*-axis (parallel to polarization) and *y*-axis

(normal to polarization) and perfectly matched layer (PML) were used for the *z*-axis (parallel to light incident direction). For single nanodisks, spectra were obtained using a total field/scattered field and by extracting the extinction cross-section of isolated PEDOT:Sulf nanodisks on a sapphire substrate. Geometry parameters are indicated in each graph (diameter, thickness, and array period) and the mesh size was typically $3 \times 3 \times 3$ nm^3, or $2 \times 2 \times 2$ nm^3 for the smaller size disks. The optical parameters for gold[33], glass[34] and PMMA[35,36] were taken from literature while the permittivities of sapphire substrate and PEDOT:Sulf were determined by ellipsometry. In the analytical calculations, the effective permittivity of the surroundings was calculated based on an average refractive index of air and sapphire ($\varepsilon_s = [(n_{air} + n_{sapphire})/2]^2$). The refractive index of sapphire is 1.75 at about 1 μm and 1.6 at about 5 μm and for simplicity we fix $n_{sapphire}$=1.6 which gives ε_s=1.69.

References

30 Brooke, R. *et al.* Vapor phase synthesized poly (3, 4-ethylenedioxythiophene)-trifluoromethanesulfonate as a transparent conductor material. *Journal of Materials Chemistry A* **6**, 21304-21312 (2018).

31 Kühne, P. *et al.* Advanced Terahertz Frequency-Domain Ellipsometry Instrumentation forIn SituandEx SituApplications. *IEEE Transactions on Terahertz Science and Technology* **8**, 257-270 (2018).

32 Tompkins, H. & Irene, E. A. *Handbook of Ellipsometry*. (William Andrew, 2005).

33 Weaver, J. H. & Frederikse, H. P. R. Optical properties of metals and semiconductors. *CRC Handbook of Chemistry and Physics* **74**, 1993-1994 (1993).

34 Philipp, H. R. in *Handbook of Optical Constants of Solids* 749-763. (Elsevier, 1997).

35 Tsuda, S., Yamaguchi, S., Kanamori, Y. & Yugami, H. Spectral and angular shaping of infrared radiation in a polymer resonator with molecular vibrational modes. *Optics Express* **26**, 6899-6915 (2018).

36 Beadie, G., Brindza, M., Flynn, R. A., Rosenberg, A. & Shirk, J. S. Refractive index measurements of poly (methyl methacrylate)(PMMA) from 0.4–1.6 μm. *Applied Optics* **54**, F139-F143 (2015).